Polymer 62 (2015) 118–128

Contents lists available at ScienceDirect

Polymer

journal homepage: www.elsevier.com/locate/polymer

Influence of the average surface roughness on the formation of superhydrophobic polymer surfaces through spin-coating with hydrophobic fumed silica

Cagla Kosak Söz, Emel Yilgör, Iskender Yilgör*

KUYTAM Surface Science and Technology Center, Chemistry Department, Koc University, Istanbul, Turkey

ARTICLE INFO

Article history:
Received 21 October 2014
Received in revised form
3 February 2015
Accepted 18 February 2015
Available online 25 February 2015

Keywords:
Superhydrophobicity
Fumed silica
Surface roughness

ABSTRACT

Formation of superhydrophobic polymer surfaces were investigated through successive spin-coating of hydrophobic fumed silica dispersed in an organic solvent onto polymer films. Two different polymers, a hydrophobic segmented silicone-urea copolymer (TPSC) and hydrophilic poly(methyl methacrylate) (PMMA) were used as model substrates. Influence of the polymer type and structure, silica concentration and the number of silica layers applied on the topography, average roughness and the wetting behavior of the surfaces were determined. Polymer surfaces obtained were characterized by scanning electron microscopy, white light interferometry, atomic force microscopy and advancing and receding water contact angle measurements. It was possible to obtain superhydrophobic surfaces displaying hierarchical micro/nano features both for TPSC and PMMA. A close correlation was observed between the number of silica layers applied and average surface roughness obtained. It was demonstrated that an average surface roughness value of 125–150 nm was necessary for the formation of superhydrophobic surfaces, both for TPSC and PMMA. Chemical structure and nature of the polymeric substrate seem to play a significant role on the topography and average roughness of the silica coated surfaces formed. Superhydrophobic surfaces displayed static and advancing water contact angles well above 150° and fairly small contact angle hysteresis.

1. Introduction

Preparation and characterization of polymeric materials with superhydrophobic surfaces have been extensively investigated during the last 15 years, after the detailed description of the surface structure of various natural plant leaves, including the lotus leaf by Barthlott and Neinhus in 1997 [1,2]. One of the main reasons for such a remarkable interest in superhydrophobic surfaces is their very interesting behavior, which include, self-cleaning, anti-fouling, stain-resistant and ice-repellant properties [3–5]. Such properties make these materials applicable in a wide range of diversified fields, including paints and coatings, textiles, exterior glass windows, rooftops, windshields, solar panels, aircraft wings and wind turbine blades [3,4,6,7]. It is well documented that the wetting behavior of a surface is controlled both by its chemical structure and the surface topography or roughness [8–10]. One of the best known examples of a superhydrophobic surface in nature is the lotus leaf [1,2,10]. As clearly shown by scanning electron microscopy (SEM) studies, the surface of the lotus leaf is covered by irregularly distributed, micron-sized protrusions called *papilla*, which have further nanoscale roughness [1,2]. Combined with the inherent hydrophobicity of the waxy layer on the leaf, these irregularly dispersed surface structures with dual-scale roughnesses give the plant its superhydrophobicity, with static water contact angle values above 150° and fairly small contact angle hysteresis [11–17].

Theoretical explanation of the effect of surface roughness on wetting behavior has been provided by Wenzel [18] and Cassie and Baxter [19]. Wenzel assumed complete wetting of the rough surface by the liquid droplet and modified the contact angle measured on a rough surface ($\cos\theta_W$) by introducing a roughness factor (r) as shown in Eqn. 1. (r) is defined as the ratio of the actual area of a rough surface to its projected geometric area and therefore its value is always greater than 1.

$$\cos\theta_W = r \cdot \cos\theta \quad (1)$$

* Corresponding author. Tel.: +90 212 338 1418; fax: +90 212 338 1559.
E-mail address: iyilgor@ku.edu.tr (I. Yilgör).

http://dx.doi.org/10.1016/j.polymer.2015.02.032
0032-3861/

Cassie–Baxter correlated the apparent contact angle (θ_{CB}) on a rough surface to the weighted average of the cosines of the contact angles on the solid and air surfaces (Eqn. 2), where (f) is defined as the fraction of the surface on top of the protrusions, $(1 - f)$ the fraction of air pockets and (θ_g) the contact angle on the air in the valleys [20]. When the contact angle of air pockets is taken as 180°, the Cassie–Baxter relationship is given by Eqn. 3.

$$\cos\theta_{CB} = f \cdot \cos\theta + (1 - f) \cdot \cos\theta_g \quad (2)$$

$$\cos\theta_{CB} = f \cdot \cos\theta + f - 1 \quad (3)$$

By combining the Cassie–Baxter and Wenzel relationships, a general equation is obtained for the apparent contact angles measured on a rough surface (θ_R).

$$\cos\theta_R = r \cdot f \cdot \cos\theta + f - 1 \quad (4)$$

As can be easily deduced from Eqn. 4, increased surface roughness will lead to much higher contact angles for hydrophobic surfaces that have a contact angle >90° on flat surfaces. There are various reports, where modified versions of these equations were developed to better explain the contact angle behavior of rough surfaces [21–24].

Due to the remarkable interest in superhydrophobicity, there have been intense efforts on developing new methods and processes for the preparation of superhydrophobic surfaces that display dual micro/nano roughness by employing a wide variety of techniques, which include; layer by layer (LBL) deposition [25], electrospinning [26], microphase separation [20,27,28], etching [29,30], spin-coating or dip-coating [20,31,32], sol–gel synthesis [10,33], surface modified silica deposition [34–36], templating [20,28,37], spraying [5,38,39] and others [10,16,20,29,30,40]. However, most of the methods described in the literature are fairly complex and may involve many steps and in general can only be applied to specific polymers. Recently we reported a fairly simple method for the preparation of polymeric materials with controlled wettability [31,32]. The method is based on spin coating of a fumed silica dispersion on a wide range of polymeric materials, thermoplastic or thermoset. It has been shown that with this simple process it was possible to prepare superhydrophobic polymer surfaces with static water contact angles greater than 170° [32]. Very interestingly, although the dramatic effects of the particle geometry or feature shape and size and distribution of protrusions on surface roughness and superhydrophobicity have been extensively discussed, no direct correlation between the experimental values of the average surface roughness and values of water contact angles or contact angle hysteresis were provided in the literature [20,30,41,42].

One of the main goals of this study was to investigate the effect of the layer-by-layer spin coating of hydrophobic fumed silica on the surface coverage, particle size and distribution, surface topography and average roughness of the surfaces obtained. Furthermore, we were especially interested in finding out if there was a critical or threshold value for the average surface roughness in order to obtain superhydrophobic surfaces. For this purpose two polymers different in nature, an inherently hydrophobic segmented silicone-urea copolymer (TPSC) and hydrophilic PMMA were chosen as the polymeric substrates. Polymer surfaces obtained were characterized by a wide range of complementary techniques which included, field emission scanning electron microscopy (FESEM), white light interferometry (WLI), static, advancing and receding water contact angle (CA) measurements, in order to gain a better understanding on the formation of superhydrophobic surfaces.

2. Experimental

2.1. Materials

Segmented thermoplastic polydimethylsiloxane-urea copolymer (Geniomer TPSC 140) (TPSC) with a PDMS content of about 92% by weight and the hydrophobic fumed silica (HDK H2000) were kindly provided by Wacker Chemie, Munich, Germany [43]. Poly(methyl methacrylate) (PMMA) (M_n = 190,000 g/mol) was synthesized in our laboratories. Primary particle size for the hydrophobic silica is reported to be 5–30 nm, which increases to 100–250 nm after aggregation. The specific surface area is 170–230 m^2/g [43]. Reagent grade isopropanol (IPA), tetrahydrofuran (THF) and toluene were obtained from Merck and were used as received.

2.2. Sample preparation

Samples were prepared through a successive or multi-step spincoating process, which was explained in detail previously [31,32]. TPSC solution was prepared in IPA, whereas the PMMA solution was prepared in toluene at concentrations of 15% and 10% by weight respectively. Silica was dispersed in THF or THF/toluene (5/2 by volume) mixture at a concentration of 0.5% and 1.0% by weight respectively. To obtain a homogeneous distribution, the dispersion was subjected to ultrasound sonication at a frequency of 35 kHz on a Sonorex RK 255H type ultrasonic bath (Bandelin, Berlin, Germany) for 10 h. Dynamic light scattering (DLS) measurements on hydrophobic silica suspensions in THF indicated fairly homogeneous distribution of the nanoparticles, with a number average size distribution of 44 ± 9 nm, which is in very good agreement with the supplier's specifications.

Glass slides (20 × 20 × 0.15 mm) were used as the substrate for spincoated films. Coating procedure was as follows: Glass slide surfaces were cleaned by wiping with IPA and THF successively several times and the parent polymer solution (TPSC or PMMA) was spincoated to obtain a film with a thickness of 20–30 μm. TPSC surfaces were coated using the silica dispersion in THF at a concentration of 0.5% by weight, while PMMA was coated by using a 1% by weight silica dispersion in THF/toluene (5/2 by volume) mixture. In each case 8 drops of silica dispersion were placed onto the base polymer film and were allowed to wet the film surface for 1 min in order to achieve efficient penetration of silica particles into the polymer during the spin coating process. Spin coating process was performed at 1000 rpm for 70 s. Before applying the subsequent layer, the coating was dried under a mild air flow at room temperature for 3 min. These steps were repeated until the desired number of silica coatings were achieved. To improve the durability of the surfaces formed, a final silica coating was applied which also contained the parent polymer. The ratio of the parent polymer to the silica in dispersion was 1/10 by weight. All samples were first dried in the hood for several hours and then in a vacuum oven at room temperature overnight. Table 1 provides the description of the sample preparation and the coding of the samples obtained, where the first four letters indicate the base polymer and (X) the number of silica layers spin coated on the film. For example TPSC-7

Table 1
Description of process parameters used for sample preparation.

Sample code	Solvent for polymer	Conc. polymer soln. (wt %)	Solvent for silica dispersion	Conc. silica dispersion (wt %)
TPSC-X	IPA	15	THF	0.5
PMMA-X	Toluene	10	THF/Toluene (5/2 by wt)	1.0

indicates a polydimethylsiloxane-urea film with 7 layers of silica coating from 0.5% by weight solution in THF.

2.3. Characterization methods

Spin-coating was performed on a Model 7600 Spin Coater by Specialty Coating Systems, Inc., Indianapolis, IN, USA. Dynamic light scattering (DLS) measurements on silica dispersions were performed on Malvern ZetaSizer Nano-S Instrument with the Nano-S software. Sample holders were glass cuvettes with square apertures.

Static water contact angle measurements were performed on a Dataphysics OCA 35 instrument at room temperature (24 ± 2 °C). 10 μL deionized, triple distilled water was used and an average of at least 10 contact angle readings were taken for each sample on each instrument. Dataphysics OCA 35 instrument was equipped with the SCA 20 software, which provided the electronic control of the device parameters and the monitoring and measurement of the contact angles. Contact angle hysteresis measurements were also conducted on Dataphysics OCA 35 instrument by dynamic sessile drop method. A 0.5 μL water droplet was dispensed from the syringe tip to touch the surface and then the volume was gradually increased to 5 μL. In order to measure the advancing angle, the volume of the sessile drop was increased at a rate of 0.2 μL/s from 5 μL to 25 μL and the highest angle achieved was accepted as the advancing angle. Then, the volume of the water droplet was decreased from 25 μL to 5 μL with the same rate. The lowest angle was accepted as the receding contact angle after the contact line between the water droplet and the surface started to decrease with a satisfactory drop shape.

Surface structures of the samples were examined using a field-emission scanning electron microscope (FESEM) (Zeiss Ultra Plus Scanning Electron Microscope) operated at 2–10 kV. Prior to FESEM study, samples were coated with a thin gold layer of 2–3 nm to minimize charging. Surface topographies of the silica coated polymer samples were investigated by White Light Interferometry (WLI) on a Bruker Contour GT Motion 3D Microscope and Non Contact Surface Profiler at the vertical scanning interferometry (VSI) mode. WLI is a fairly sensitive technique for three dimensional surface mapping of various substrates including polymeric films, foams, textile fabrics and integrated circuit boards. Using WLI it is possible to measure feature sizes from sub nanometer to millimeter range. In VSI mode average surface roughnesses of the samples with height discontinuities between 150 nm to several mm can be precisely measured. In our studies at least 10 surface maps with dimensions of 63 × 47 μm^2 were obtained from different sections of the silica coated samples to determine the average surface roughness values. Atomic force microscope (AFM) images were obtained on a Bruker Dimension Icon Atomic Force Microscope equipped with ScanAsyst. AFM images were taken in standard tapping mode in air by using Bruker MPP-13120 silicon tip with a force constant of 375 N/m and resonance frequency of 525 kHz. For the calculation of the average surface roughness values height and phase images were obtained from several different 50 × 50 μm^2 sections on the sample surface.

3. Results and discussion

Preparation, characterization and applications of superhydrophobic surfaces have received widespread attention during the last 15 years, even though the superhydrophobic behavior of rough surfaces have been theoretically formulated by Wenzel [18] and Cassie and Baxter [19] over 70 years ago. Interestingly, the dramatic interest in the field by the experimentalists materialized after the reports on the characteristic surface morphologies and resultant superhydrophobic properties of a large number of plants [1,2]. McCarthy and co-workers [8,9,11–14,44–56] and various other groups [4,10,15–17,20,33,41,57–71] have performed some of the pioneering investigations in the field, including the experimental studies on the preparation and characterization of superhydrophobic surfaces and critical evaluation of the theoretical foundations. A large number of excellent review articles providing detailed information and discussions on various aspects of superhydrophobic surfaces are available [4,10,20,28–30,40,59,60,72].

As shown in Fig. 1, a critical feature of the lotus leaf surface revealed by scanning electron microscopy analysis was the presence of cone-like hierarchical structures with micron and nano-sized features [2]. As can be seen in Fig. 1-a, cone type protrusions with base diameters of 5–15 μm, heights of 10–50 μm and aspect ratios in 0.7–10 range, are irregularly distributed on the leaf surface with distances between each other ranging from 10 to 100 μm. As provided on the expanded image in Fig. 1-b, the secondary structure exhibited by the cones has nanometer sized hairy features, which are reported to be critical in achieving superhydrophobicity with static water contact angles >150° and low contact angle hysteresis [11–17]. In addition to lotus and various other plant leaves, such micro- and nano-sized hierarchical structures are also observed on butterfly wings and other insects [73,74].

As already discussed, a variety of techniques have been developed and utilized for the preparation of superhydrophobic polymer surfaces [10,16,20,29,30,38–40]. Unfortunately, most of these techniques are fairly tedious and can be applied to a specific group of polymers. We recently reported a simple spin-coating method using hydrophobic fumed silica, which could be applied to a wide range of polymers, thermoplastic (e.g. polystyrene, polycarbonate, polyurethane) or thermoset (epoxy resins) to produce superhydrophobic surfaces with very high static water contact angles and very low contact angle hysteresis [32]. Although all published reports extensively discussed the dramatic effect of surface roughness on superhydrophobicity, no direct correlation between

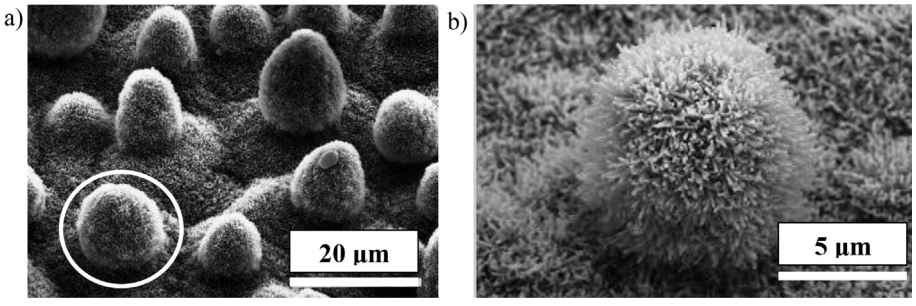

Fig. 1. SEM images of (a) surface of the lotus leaf surface and (b) enlarged view of a single papilla showing the surface nanostructure [2]. Reproduced with permission from Oxford University Press.

the experimental values of the average surface roughness and values of water contact angles or contact angle hysteresis were provided [20,42,58,75]. In this report we discuss our studies on the development of superhydrophobic surfaces through successive (or layer-by-layer) spin-coating of hydrophobic fumed silica on two inherently different polymers, a hydrophobic silicone-urea segmented copolymer (TPSC) and hydrophilic poly(methyl methacrylate) (PMMA). Effect of the number of silica layers applied on surface coverage, particle size, its distribution and average surface roughness were investigated by Field Emission Scanning Electron microscopy (SEM), White Light Interferometry (WLI) and Atomic Force Microscopy (AFM). Superhydrophobicity of the surfaces formed were demonstrated by advancing and receding water contact angle measurements and contact angle hysteresis (CAH).

3.1. Surface properties of fumed silica coated superhydrophobic silicone-urea (TPSC) copolymers

3.1.1. Scanning electron microscopy (SEM) studies

Fig. 2 provides the SEM images of uncoated and silica coated TPSC surfaces. Uncoated TPSC, which is mainly composed of extremely flexible PDMS chains, displays a very flat and featureless

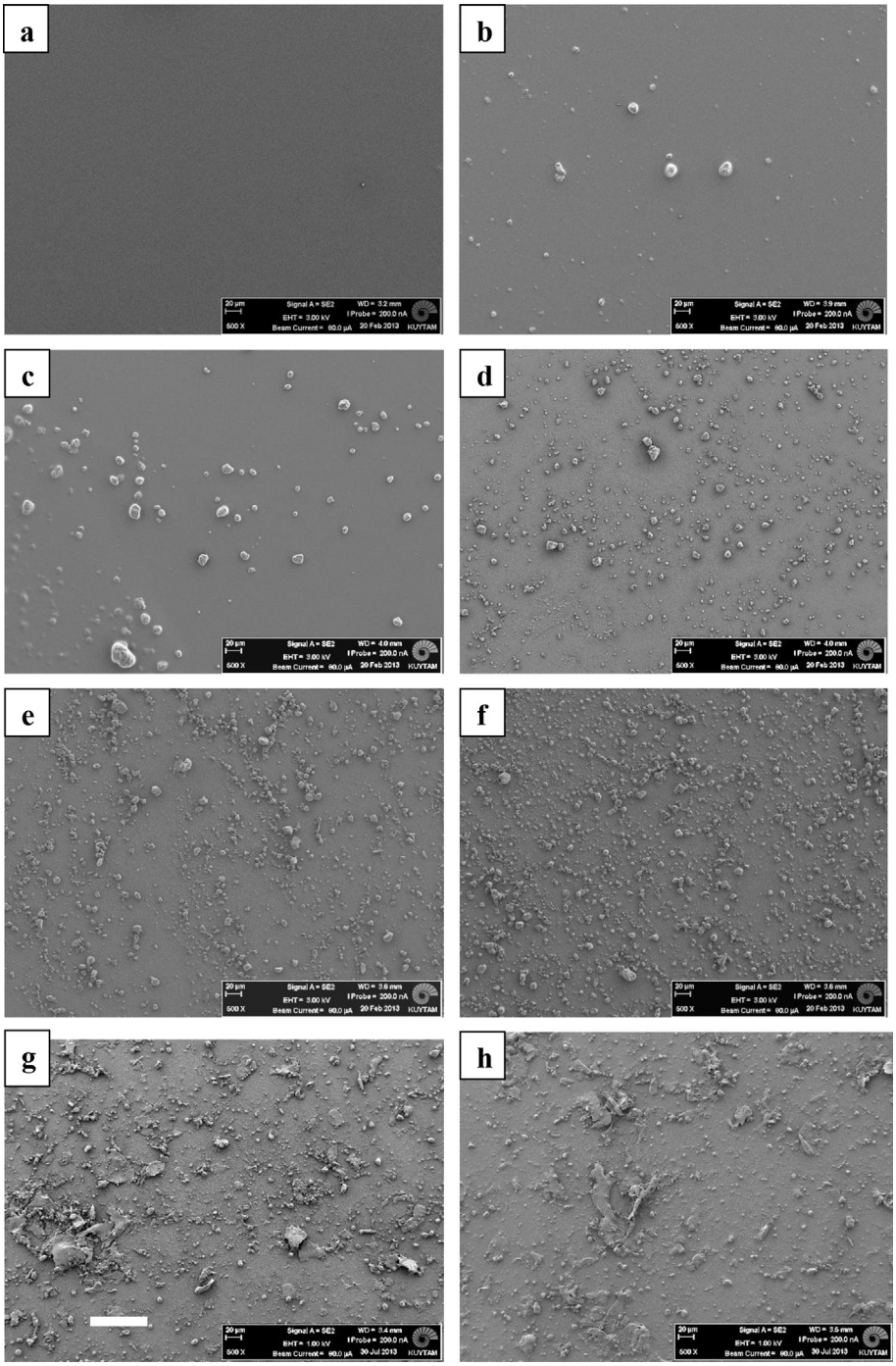

Fig. 2. SEM images of uncoated and silica spin-coated TPSC surfaces, (a) uncoated, and after (b) 1, (c) 2, (d) 3, (e) 5, (f) 6, (g) 9, and (h) 10 silica coatings (scale bar 50 μm for all samples).

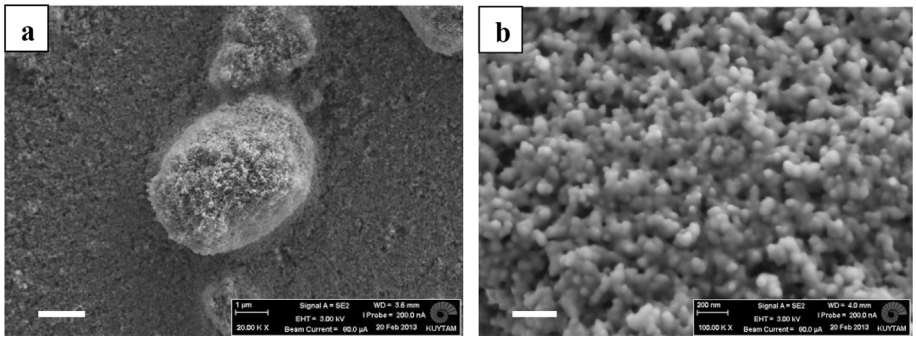

Fig. 3. SEM images of (a) an agglomerated silica particle on TPSC-6 film (scale bar 1 μm), and (b) nanostructure of the silica particle surface (scale bar 200 nm).

surface as can be seen in Fig. 2-a. Spin-coating of one layer of hydrophobic fumed silica from a very dilute 0.5% by weight dispersion in THF leads to the formation of a surface coated with highly scattered silica particles with sizes in 1–15 μm range, randomly distributed on the surface. Particle size of the silica, which on the average is around 44 ± 9 nm in THF dispersion, increases dramatically when coated on TPSC surface due to agglomeration. However, at lower coating levels, silica agglomerates are far apart from each other and lack in surface density to generate a topography, similar to that observed on lotus leaf. This pattern of insufficient coverage on the surface may be the reason that superhydrophobic behavior is not observed at low number of coating layers. As expected, the silica surface coverage increases as a function of the number of coatings applied, without a noticeable change in the particle size until 8 layers of coating (Fig. 2b–f).

Very interestingly, as shown in Fig. 2g and h, sizes of the silica particles increase dramatically after 9 and 10 spin-coating applications, most probably due to the saturation of the surface and

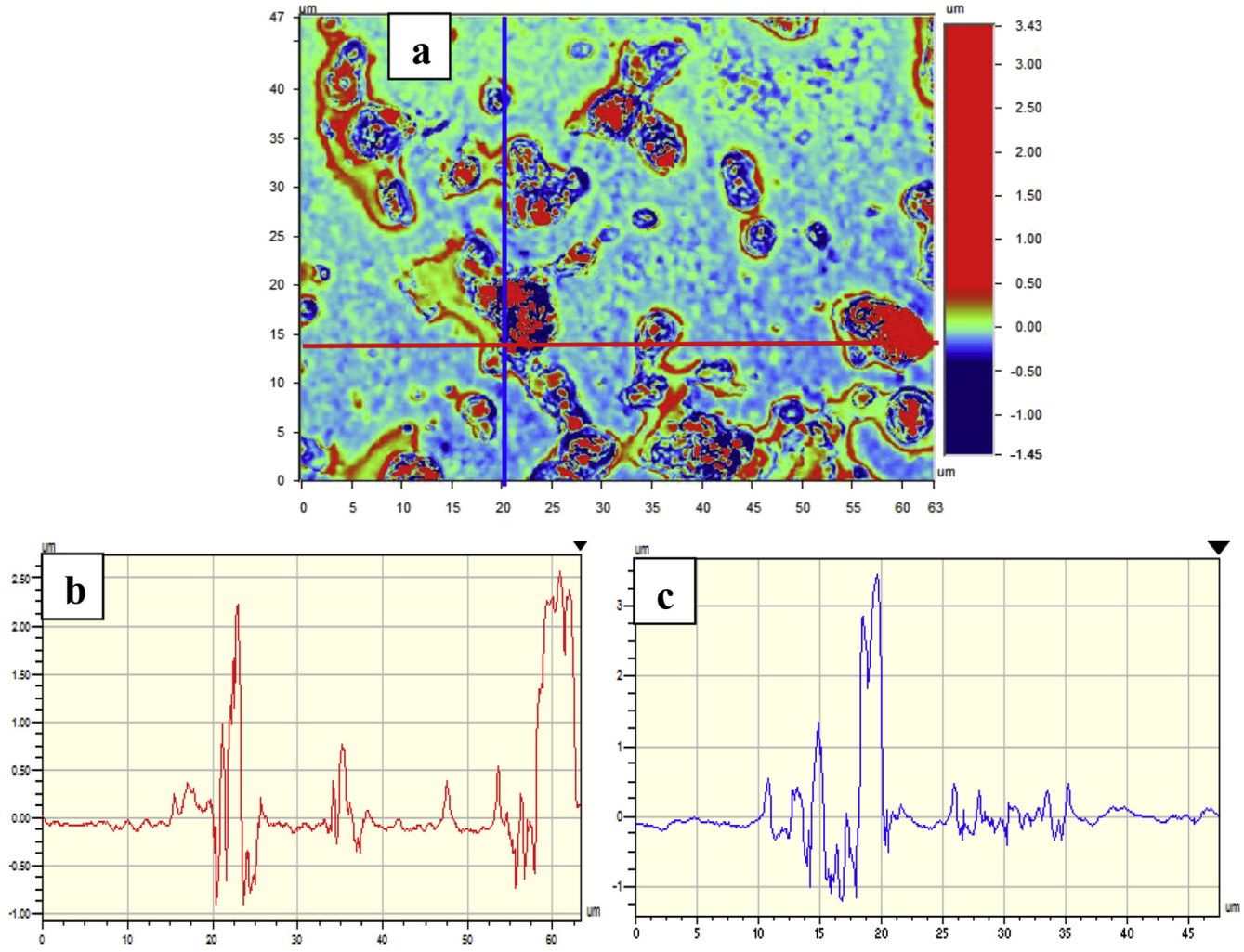

Fig. 4. Surface analysis of silica coated TPSC-6 by White Light Interferometry. (a) 2D Topographical image of 47 × 63 μm^2 sample surface and depth profiles of surfaces along, (b) X-axis and (c) Y-axis.

Table 2
Average surface roughness, static, advancing and receding water contact angles and contact angle hysteresis values, as a function of the number of coatings applied, for TPSC samples spin-coated with hydrophobic fumed silica.

Sample	Av. Roughness (nm)	Static water CA (°)	Adv. CA (°)	Rec. CA (°)	CAH (°)
TPSC	6.3 ± 1.1	110.5 ± 0.5	117.0 ± 1.1	93.6 ± 0.1	23.4
TPSC-1	76.6 ± 14.4	109.2 ± 0.3	102.1 ± 1.4	77.8 ± 1.2	24.3
TPSC-2	118.2 ± 13.7	108.6 ± 1.8	100.5 ± 1.7	77.6 ± 1.7	24.1
TPSC-3	124.3 ± 28.6	150.8 ± 2.1	168.6 ± 1.9	159.8 ± 9.0	8.8
TPSC-4	122.9 ± 17.2	162.9 ± 0.6	166.8 ± 1.6	165.6 ± 1.3	1.2
TPSC-5	120.9 ± 47.8	161.4 ± 2.9	168.4 ± 1.5	167.3 ± 0.8	1.1
TPSC-6	190.4 ± 37.6	159.3 ± 0.2	168.2 ± 0.4	168.1 ± 0.6	0.1
TPSC-7	208.0 ± 70.4	164.5 ± 0.1	167.9 ± 0.5	167.7 ± 0.2	0.2
TPSC-8	159.4 ± 23.7	160.0 ± 1.0	167.5 ± 0.8	167.4 ± 1.0	0.1
TPSC-9	85.9 ± 18.3	140.0 ± 0.4	156.6 ± 1.4	145.1 ± 2.4	11.5
TPSC-10	84.2 ± 19.0	143.1 ± 0.9	130.6 ± 0.2	117.6 ± 1.4	13.0

strong tendency of the particles to agglomerate to form a fused silica network. These agglomerates, which are also distorted in shape and are somewhat elongated may be responsible in deviation from Lotus-like behavior and lower static water contact angles observed, as will be discussed later. It is important to note that the surface coatings obtained by successive spin coating processes do not necessarily form independent layers, but they are more like aggregate coatings obtained by gradually depositing certain amount of fumed silica particles during each spin-coating step. As a result, the amount of surface covered by fumed silica particles increases with the number of spin-coating steps.

As already discussed, one of the critical features of naturally superhydrophobic surfaces is the presence of micro- and nano-sized hierarchical structures in the particles. SEM micrographs provided on Fig. 2 suggest that the aggregated fumed silica particles most probably are also percolated, providing a topography with micro and nano length-scales suitable for entrapping air and thus generating superhydrophobic surfaces with very high water contact angles and low contact angle hysteresis. To demonstrate the formation of such a dual sized hierarchical structure in the silica coatings obtained, one of the particles on the TPSC-6 sample (coated with 6 spin-coating steps of silica) was randomly chosen and examined in SEM under higher magnification (20,000× and 100,000×) (Fig. 3).

SEM images, which are provided in Fig. 3, clearly demonstrate the hierarchical structure of the silica particles on the polymer surface. As can be seen in Fig. 3-a, the diameter of the agglomerated silica particle is about 5 μm, which also displays nanometer sized surface roughness as shown in Fig. 3-b. Nanosize roughness is due to the individual fumed silica particles in the aggregate, which have dimensions in 5–30 nm range [43]. Very similar micro and nano-sized hierarchical structures were observed in all silica particles investigated in all of the samples obtained, which are not shown here.

3.1.2. Average surface roughness determination

In addition to SEM studies, which provided information on the size and distribution of the silica particles, extent of surface coverage and topography of the TPSC surfaces as a function of the number of layers applied, White Light Interferometry (WLI) at Vertical Scanning Interferometry (VSI) mode was used to investigate the surface topographies of the coated samples and to determine the average surface roughness values. In addition, height and phase images and surface roughness values of a silica coated TPSC sample was also obtained by AFM for comparison.

3.1.2.1. White light interferometry (WLI). WLI is a simple, non-contact technique which provides quantitative information on the 3-dimensional surface topography of materials. It is based on the analysis of the interference patterns of light waves with a broad optical bandwidth capable of precisely mapping a variety of surfaces with roughnesses from nanometer to millimeter range. Fig. 4-a provides the WLI image of a 47 × 63 μm^2 section of the TPSC-6 surface. The colors indicate the heights (red (in web version)) and depths (blue (in web version)) of the peaks and valleys respectively, while the flat regions are in green (in web version) color as shown by the column on the left-hand-side. Depth profiles of the TPSC-6 surface along a horizontal and vertical line, as marked on Fig. 4-a, are provided in Fig. 4b and c respectively. As can be seen from these depth profiles, silica particles with heights in 2.5–3.5 μm range are randomly distributed on surfaces that display nanoroughness. Average surface roughness values determined from WLI measurements on uncoated and silica coated TPSC samples with dimensions of 47 × 63 μm^2 are provided on Table 2. Also included in Table 2 are the static water contact angles obtained on these samples.

As can be seen from Table 2, uncoated TPSC surface, is fairly smooth and has an average roughness of 6.3 ± 1.1 nm. Surface roughness of TPSC coated only with one layer of silica dramatically increases to 76.6 ± 14.4 nm. As the number of silica coatings

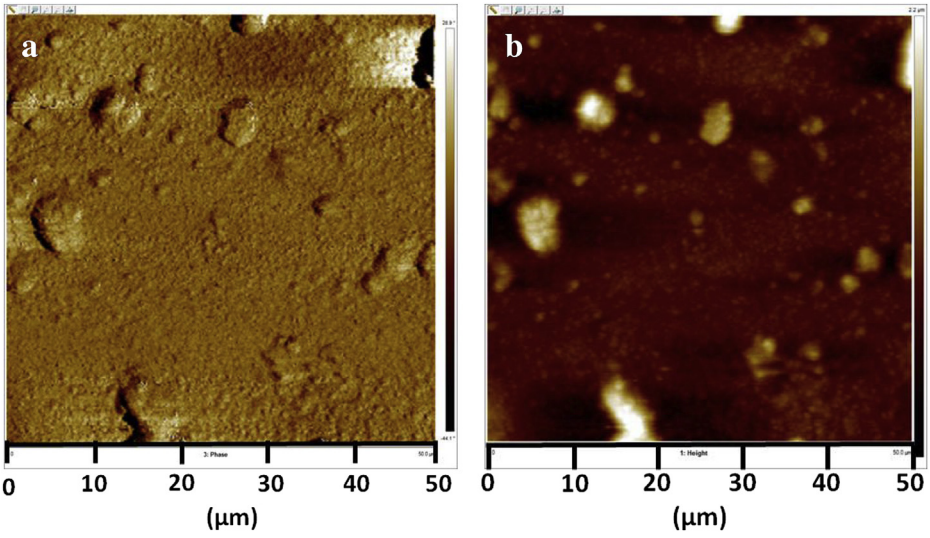

Fig. 5. AFM images of 50 × 50 μm^2 TPSC-6. (a) Phase image and (b) height image.

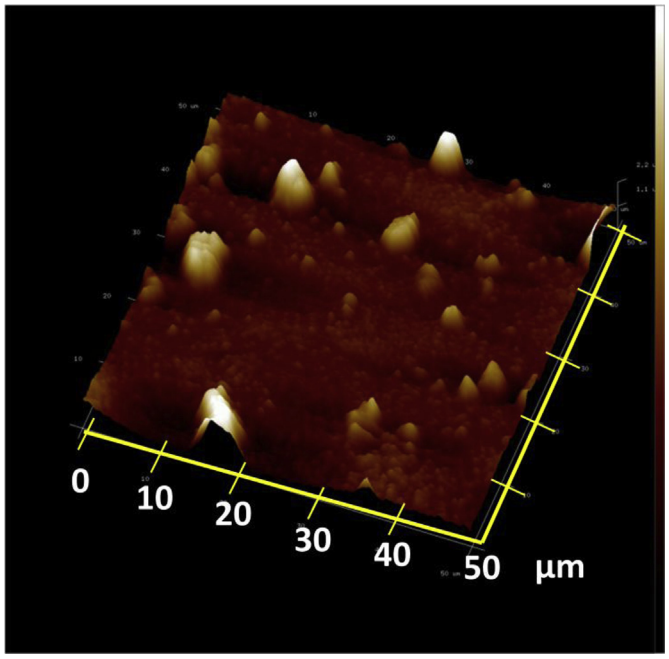

Fig. 6. 3D AFM image of 50 × 50 µm^2 TPSC-6 surface.

increase, average surface roughness also increase gradually, reaching to a maximum value of 208.0 ± 70.4 nm after 7 layers of coating. Addition of more layers results in a slight decrease in the surface roughness, which is most probably due to the maximum coverage of the surface and agglomeration of the silica particles, as can also be seen in the SEM images provided in Fig. 2.

3.1.2.2. Atomic force microscopy (AFM). Silica coated samples obtained in this study have protrusion heights of 2 to over 5 µm, which are very close to the Z-axis limit of the AFM instruments. However, since AFM is a very sensitive surface characterization technique in order to compare the results obtained by WLI, height and phase images and average surface roughness values of TPSC-4 and TPSC-6 were also obtained by AFM. In order to obtain good images a silicon tip with a very high force constant of 375 N/m and a resonance frequency of 525 kHz was used. AFM phase and height images of a 50 × 50 µm^2 TPSC-6 sample are provided on Fig. 5. For a better illustration of the surface topography, 3D AFM image of TPSC-6 surface is also reproduced on Fig. 6.

The phase image provided in Fig. 5-a is very similar to that observed by SEM, where fairly homogeneously distributed silica particles with diameters of 2 to about 10 µm are observed. In the height image (Fig. 5-b) hard silica particles are observed as light colored domains. Maximum particle height obtained was 2.2 µm. Fig. 6 clearly shows the 3D topography with silica particle heights of 0.5–2.2 µm. Particle tops look fairly sharp, which is due very hard tapping. Average surface roughness values (R_a) obtained for TPSC-4 and TPSC-6 surfaces from AFM studies were 119 and 166 nm respectively, which compare very well with the (R_a) values obtained from WLI, which are 122.9 ± 17.2 and 190.4 ± 37.6 nm as reported on Table 2.

3.1.3. Water contact angle measurements and contact angle hysteresis studies on TPSC samples

Average values of the static, advancing and receding water contact angles and contact angle hysteresis obtained on the uncoated and hydrophobic fumed silica coated TPSC surfaces are provided in Table 2 as a function of the number of coatings applied from a very dilute dispersion of 0.5% by weight silica in THF.

Since uncoated TPSC surface is mainly covered with PDMS, it is relatively hydrophobic and displays a static water contact angle of 110.5 ± 0.5°, typical for PDMS surfaces. Contact angles of TPSC samples coated with 1 and 2 layers of silica do not show any noticeable change. On the other hand TPSC-3 sample which has 3 layers of silica coating shows a dramatically higher contact angle of 150.8 ± 2.1°, which indicates formation of a superhydrophobic surface. Addition of more silica layers gradually increase the water contact angle, which reaches to a plateau with contact angle values between 160 and 165°, well above the critical value of 150°, reported to be necessary for superhydrophobic behavior. Application of more layers of silica coating do not provide any further improvement, but leads to a slow decrease in the static water contact angle to around 140°, parallel to the decrease in the surface roughness as shown on Table 2. As can be seen from Table 2, we believe one of the critical observations on hydrophobic fumed silica coated TPSC copolymers investigated in this study, is the formation of superhydrophobic surfaces with water contact angles of >150° only when the average surface roughness of the samples reach to around 120 nm.

Another critical parameter strongly supporting superhydrophobicity is the contact angle hysteresis (CAH), which is the difference between the advancing and receding contact angles. It is suggested that for a truly superhydrophobic surface CAH should be < 10°, where water droplets would roll effortlessly on the

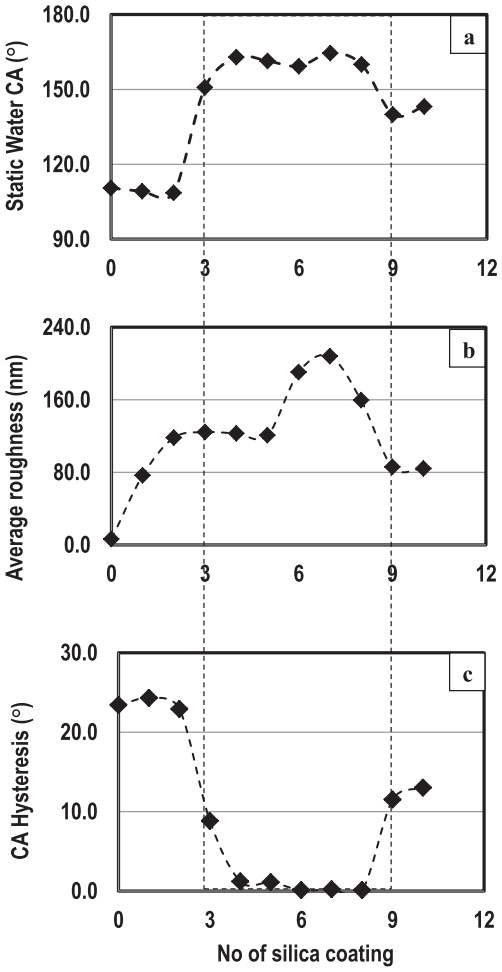

Fig. 7. Relationship between; (a) the static water contact angles, (b) average surface roughness, and (c) contact angle hysteresis values as a function of the number of silica spin-coating applied onto TPSC.

surface, without pinning [53]. Table 2 provides the advancing and receding water contact angles and CAH data for TPSC samples. It is interesting to note the fairly high CAH values around 24° for uncoated TPSC and samples coated with 1 and 2 layers of silica, which also displayed somewhat low static water contact angles around 110°. On the other hand TPSC-3, which has a static water contact angle of 150.8 ± 2.1° also has a fairly low CAH value of 8.8° clearly indicating the formation of a superhydrophobic surface. CAH values decrease dramatically to 1° or lower as the number of silica coating layers increases. Fig. 7a and b provide the variation in the static water contact angles and CAH values respectively, as a function of the number of silica spin-coatings applied onto the TPSC surface. Both data clearly indicate the formation of superhydrophobic surfaces after 3 silica spin-coating steps, with static water contact angles above 150° and CAH values well below 10°.

For a better visualization of the relationship between the change in the surface roughness and its influence on the static water contact angles and on contact angle hysteresis of silica coated TPSC surfaces, the data presented in Table 2 are plotted in Fig. 7. The shaded area in Fig. 7 clearly demonstrates the strong interdependency between the increased surface roughness, very high static water contact angles of around 160° and extremely low CAH values on superhydrophobic TPSC surfaces obtained by the successive spin-coating of fumed silica. However, it is also important to note

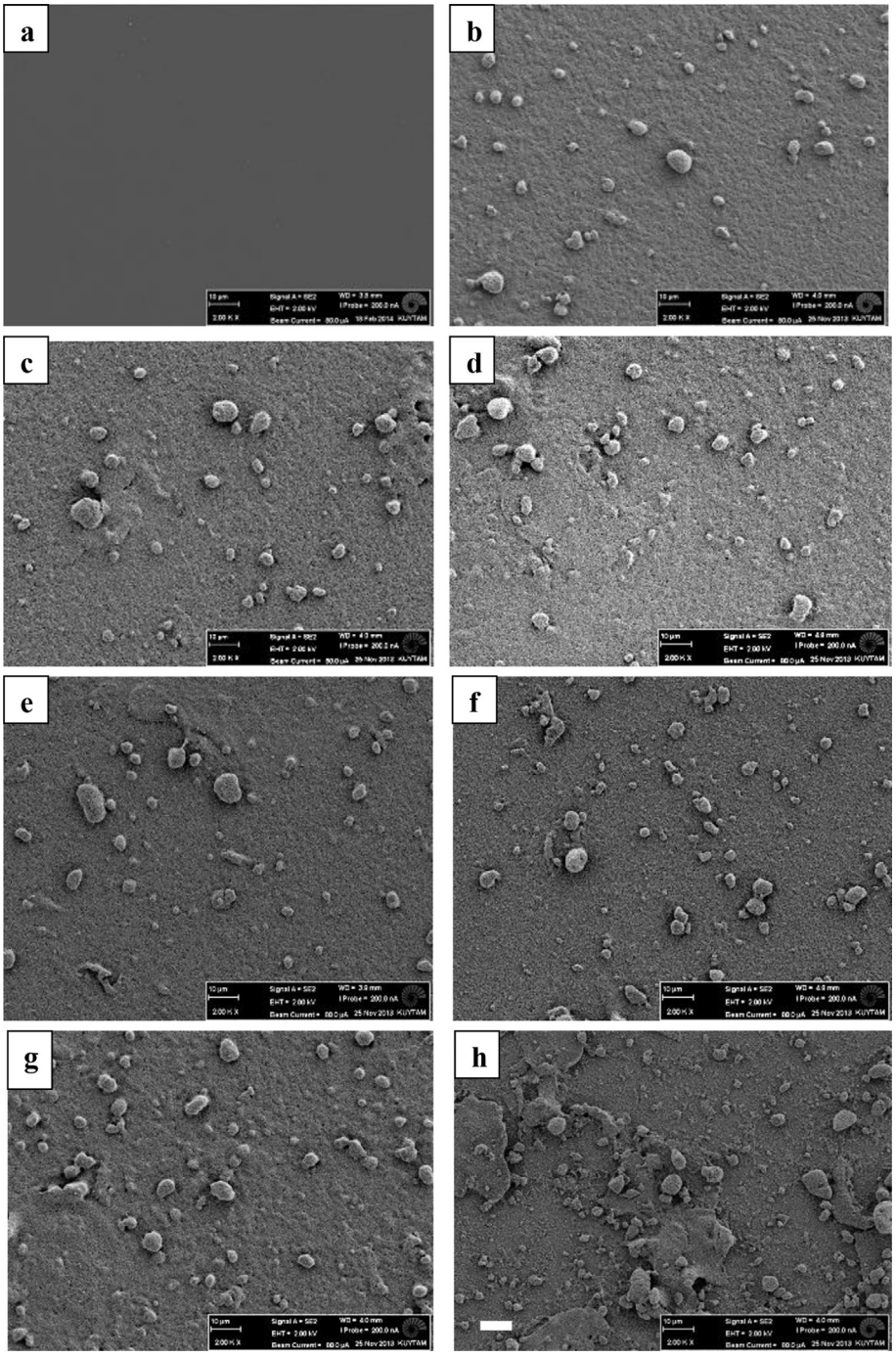

Fig. 8. SEM images of uncoated and silica spin-coated PMMA surfaces, (a) uncoated, and after (b) 1, (c) 2, (d) 3, (e) 4, (f) 7, (g) 9, and (h) 10 silica coatings (scale bar 10 μm).

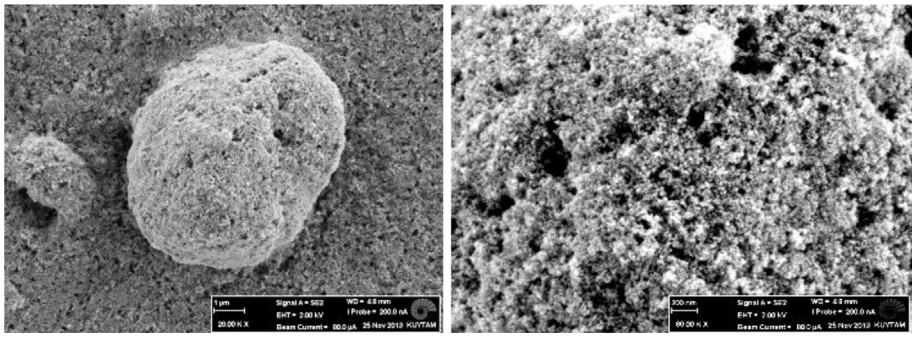

Fig. 9. SEM images of a silica particle on PMMA surface after 7 spin-coating steps, showing the formation of a micro-nano hierarchical structure.

that in addition to a critical roughness value, in order to obtain superhydrophobic behavior the surface must also be homogeneously covered with agglomerated silica particles that are separated from each other in 10–50 μm range as observed in SEM studies shown in Fig. 2.

3.2. Surface properties of fumed silica coated poly(methyl methacrylate) (PMMA)

In addition to inherently hydrophobic TPSC, we also investigated the preparation of superhydrophobic surfaces through layer by layer spin coating of hydrophobic, fumed silica on inherently hydrophilic PMMA, which has an average static water contact angle of 67.5 ± 0.7°. For this purpose 1% silica dispersion in THF/toluene (5/2 by weight) was used as the coating mixture. Similar to TPSC systems, PMMA surfaces were characterized by SEM, WLI, static, advancing and receding water contact angle measurements.

SEM images of the uncoated and various layers of silica coated PMMA surfaces are provided in Fig. 8. As expected, uncoated PMMA surface (Fig. 8-a) is fairly smooth and featureless. Application of just one layer of fumed silica coating from 1% dispersion results in the formation of a fairly homogeneous silica coating over the PMMA surface with particle size varying in 1–10 μm range (Fig. 8-b). Application of more layers of silica leads to an increase in the number of particles covering the surface but does not seem to influence the average particle size until about 9 spin-coating steps (Fig. 8-c, d). Similar to the observations made on TPSC surfaces, application of 9 and especially 10 layers of coating results in the agglomeration of silica particles. This leads to the formation of microplaques in sizes ranging from 20 to 50 μm. As can be seen in Fig. 8-f, some of these microplaques are also interconnected and form larger surface structures.

As shown in Fig. 9, when a typical silica particle on the PMMA surface is examined under higher magnification, surface nanostructure is clearly visible, indicating the formation of a micro-nano hierarchical structure, similar to those observed for TPSC surfaces and the Lotus leaf.

3D Roughness profiles and average surface roughness values of the silica coated PMMA surfaces were also determined by using WLI. Results obtained are summarized on Table 3 together with the average static, advancing and receding contact angles and CAH values obtained on these surfaces. When compared with TPSC surfaces, the roughness values of PMMA surfaces are generally much higher at the same number of silica coating layers. This is most probably due to the higher concentration of the fumed silica in the dispersion used for the spin-coating process and the hydrophilic nature of PMMA surface, which does not interact strongly with the hydrophobic silica particles. This leads to aggregation of the hydrophobic silica particles during spin coating and results in formation of larger silica particles and a coating with higher roughness. Unlike the TPSC system, where superhydrophobic surfaces were obtained after 3 layers of coating, in PMMA static and advancing water contact values of 150 and 161.5° were obtained after only one layer of coating. Average values of the static and advancing water contact angles did not display much change as a function of the number of silica coating layers applied. When compared with the values obtained on TPSC surfaces in superhydrophobic regime, PMMA surfaces display slightly higher CAH values in 0.2–15.6° range, which most probably is due to pinning on highly irregular surface topography which is generally made of larger silica agglomerates.

Fig. 10 provides the change in the surface roughness as a function of the number of silica spin-coating steps applied and its influence on the static water contact angles and contact angle hysteresis of silica coated PMMA surfaces, which is generated by using the data presented in Table 3. These results on PMMA, which is an inherently hydrophilic surface are very similar to those obtained on hydrophobic TPSC surfaces provided in Fig. 7 indicating no significant effect of the nature of the uncoated film on the silica coated superhydrophobic surfaces obtained.

4. Conclusions

Preparation and characterization of superhydrophobic polymer surfaces have received widespread attention during the last 15 years. This led to the development of a large number of methods and processes for their preparation, which included electrospinning, etching, microphase separation, spraying, sol–gel synthesis and various other techniques [16,20]. Unfortunately, most of these techniques are substrate specific and usually involve fairly tedious processes. In this study a simple method, which is based on successive spin-coating of a hydrophobic fumed silica dispersion in an organic solvent onto a silicone-urea (TPSC) copolymer or

Table 3
Average surface roughness, static, advancing and receding water contact angles and contact angle hysteresis values as a function of the number of coatings applied for PMMA samples spin-coated with fumed silica.

Sample code	Av. Rough. (nm)	Static water CA (°)	Advancing CA (°)	Receding CA (°)	CAH (°)
PMMA	13.3 ± 5.7	67.5 ± 0.7	72.9 ± 1.5	51.7 ± 0.6	21.2
PMMA-1	190.0 ± 50.2	149.6 ± 0.8	160.3 ± 1.8	151.4 ± 1.4	8.9
PMMA-2	173.3 ± 89.3	149.7 ± 4.7	159.9 ± 0.6	149.6 ± 1.6	10.3
PMMA-3	202.8 ± 54.2	148.1 ± 2.3	162.8 ± 1.9	149.0 ± 1.3	13.8
PMMA-4	201.8 ± 53.1	147.7 ± 2.9	161.3 ± 0.9	145.7 ± 0.6	15.6
PMMA-5	300.9 ± 131.9	156.0 ± 0.2	160.2 ± 0.4	150.6 ± 1.1	9.6
PMMA-6	386.3 ± 88.2	166.0 ± 0.4	166.7 ± 0.6	166.0 ± 1.1	0.7
PMMA-7	313.9 ± 86.7	168.2 ± 0.8	169.9 ± 0.8	169.7 ± 0.4	0.2
PMMA-8	249.5 ± 82.3	163.1 ± 0.4	162.8 ± 0.2	157.3 ± 1.8	5.5
PMMA-9	132.4 ± 18.0	163.5 ± 0.2	165.0 ± 0.6	158.4 ± 1.4	6.6
PMMA-10	183.0 ± 52.7	151.3 ± 0.6	157.7 ± 1.6	148.8 ± 1.8	8.9

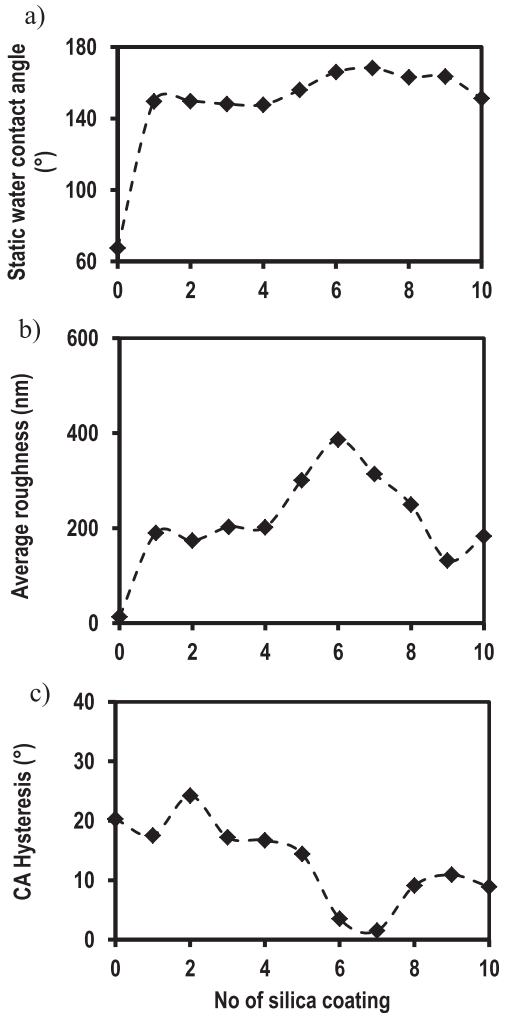

Fig. 10. Relationship between; (a) the static water contact angles, (b) average surface roughness, and (c) contact angle hysteresis values as a function of the number of silica spin-coating applied onto PMMA.

poly(methyl methacrylate) (PMMA) film surface has been described for the preparation of superhydrophobic polymer surfaces. SEM studies have shown the formation of surface topographies with hierarchical micro-nano features both for TPSC and PMMA samples, which is reported to be critical in obtaining superhydrophobic behavior [16,49,57,58]. Average surface roughness values have been shown to increase from about 10 nm for the uncoated base film to greater than 300 nm as a function of the number of silica layers applied, using White Light Interferometry and Atomic Force Microscopy measurements. TPSC and PMMA surfaces displayed superhydrophobic behavior with static water contact angles well above 150° and contact angle hysteresis values below 10° when the average surface roughness values reach around 125–150 nm.

References

[1] Barthlott W, Neinhuis C. Purity of the sacred lotus, or escape from contamination in biological surfaces. Planta 1997;202(1):1–8.
[2] Neinhuis C, Barthlott W. Characterization and distribution of water-repellent, self-cleaning plant surfaces. Ann Bot 1997;79(6):667–77.
[3] Verho T, Bower C, Andrew P, Franssila S, Ikkala O, Ras RHA. Mechanically durable superhydrophobic surfaces. Adv Mater 2011;23(5):673–8.
[4] Nosonovsky M, Bhushan B. Superhydrophobic surfaces and emerging applications: non-adhesion, energy, green engineering. Curr Opin Colloid & Interface Sci 2009;14(4):270–80.
[5] Manoudis PN, Karapanogiotis I, Tsakalof A, Zuburtikudis I, Panayiotou C. Superhydrophobic composite films produced on various substrates. Langmuir 2008;24(19):11225–32.
[6] Peng CY, Xing SL, Yuan ZQ, Xiao JY, Wang CQ, Zeng JC. Preparation and anticing of superhydrophobic PVDF coating on a wind turbine blade. Appl Surf Sci 2012;259:764–8.
[7] Manoudis PN, Karapanogiotis I, Tsakalof A, Zuburtikudis I, Kolinkeova B, Panayiotou C. Surface properties of superhydrophobic coatings for stone protection. J Nano Res 2009;8:23–33.
[8] Gao LC, McCarthy TJ. The "lotus effect" explained: two reasons why two length scales of topography are important. Langmuir 2006;22(7):2966–7.
[9] Oner D, McCarthy TJ. Ultrahydrophobic surfaces. Effects of topography length scales on wettability. Langmuir 2000;16(20):7777–82.
[10] Bhushan B, Jung YC. Natural and biomimetic artificial surfaces for superhydrophobicity, self-cleaning, low adhesion, and drag reduction. Prog Mater Sci 2011;56(1):1–108.
[11] Chen W, Fadeev AY, Hsieh MC, Oner D, Youngblood J, McCarthy TJ. Ultrahydrophobic and ultralyophobic surfaces: some comments and examples. Langmuir 1999;15(10):3395–9.
[12] Takeshita N, Paradis L, Oner D, McCarthy TJ, Chen W. Simultaneous tailoring of surface topography and chemical structure for controlled wettability. Langmuir 2004;20(19):8131–6.
[13] Gao LC, McCarthy TJ. Contact angle hysteresis explained. Langmuir 2006;22(14):6234–7.
[14] Krumpfer JW, McCarthy TJ. Contact angle hysteresis: a different view and a trivial recipe for low hysteresis hydrophobic surfaces. Faraday Discuss 2010;146:103–11.
[15] Jung YC, Bhushan B. Contact angle, adhesion and friction properties of micro- and nanopatterned polymers for superhydrophobicity. Nanotechnology 2006;17(19):4970–80.
[16] Koch K, Bhushan B, Jung YC, Barthlott W. Fabrication of artificial Lotus leaves and significance of hierarchical structure for superhydrophobicity and low adhesion. Soft Matter 2009;5(7):1386–93.
[17] McHale G, Shirtcliffe NJ, Newton MI. Contact-angle hysteresis on superhydrophobic surfaces. Langmuir 2004;20(23):10146–9.
[18] Wenzel RN. Resistance of solid surfaces to wetting by water. Ind Eng Chem 1936;28:546–51.
[19] Cassie ABD, Baxter S. Wettability of porous surfaces. Trans Faraday Soc 1944;40:546–51.
[20] Roach P, Shirtcliffe NJ, Newton MI. Progress in superhydrophobic surface development. Soft Matter 2008;4(2):224–40.
[21] Onda T, Shibuichi S, Satoh N, Tsujii K. Super-water-repellent fractal surfaces. Langmuir 1996;12(9):2125–7.
[22] Extrand CW. Contact angles and hysteresis on surfaces with chemically heterogeneous islands. Langmuir 2003;19(9):3793–6.
[23] Extrand CW. Model for contact angles and hysteresis on rough and ultraphobic surfaces. Langmuir 2002;18(21):7991–9.
[24] Erbil HY, Cansoy CE. Range of applicability of the Wenzel and Cassie-Baxter equations for superhydrophobic surfaces. Langmuir 2009;25(24):14135–45.
[25] Bravo J, Zhai L, Wu ZZ, Cohen RE, Rubner MF. Transparent superhydrophobic films based on silica nanoparticles. Langmuir 2007;23(13):7293–8.
[26] Acatay K, Simsek E, Ow-Yang C, Menceloglu YZ. Tunable, superhydrophobically stable polymeric surfaces by electrospinning. Angew Chem Int Ed 2004;43(39):5210–3.
[27] Han JT, Xu XR, Cho KW. Diverse access to artificial superhydrophobic surfaces using block copolymers. Langmuir 2005;21(15):6662–5.
[28] Yan YY, Gao N, Barthlott W. Mimicking natural superhydrophobic surfaces and grasping the wetting process: a review on recent progress in preparing superhydrophobic surfaces. Adv Colloid Interface Sci 2011;169(2):80–105.
[29] Shirtcliffe NJ, McHale G, Atherton S, Newton MI. An introduction to superhydrophobicity. Adv Colloid Interface Sci 2010;161(1–2):124–38.
[30] Ma ML, Hill RM. Superhydrophobic surfaces. Curr Opin Colloid & Interface Sci 2006;11(4):193–202.
[31] Yilgör I, Bilgin S, Isik M, Yilgör E. Tunable wetting of polymer surfaces. Langmuir 2012;28(41):14808–14.
[32] Yilgör I, Bilgin S, Isik M, Yilgör E. Facile preparation of superhydrophobic polymer surfaces. Polymer 2012;53(6):1180–8.
[33] Shirtcliffe NJ, McHale G, Newton MI, Perry CC, Roach P. Superhydrophobic to superhydrophilic transitions of sol-gel films for temperature, alcohol or surfactant measurement. Mater Chem Phys 2007;103(1):112–7.
[34] Deng X, Mammen L, Butt HJ, Vollmer D. Candle soot as a template for a transparent robust superamphiphobic coating. Science 2012;335(6064):67–70.
[35] Deng X, Mammen L, Zhao YF, Lellig P, Müllen K, Li C, et al. Transparent, thermally stable and mechanically robust superhydrophobic surfaces made from porous silica capsules. Adv Mater 2011;23(26):2962.
[36] Mammen L, Deng X, Untch M, Vijayshankar D, Papadopoulos P, Berger R, et al. Effect of nanoroughness on highly hydrophobic and superhydrophobic coatings. Langmuir 2012;28(42):15005–14.
[37] Zhang L, Zhou ZL, Cheng B, DeSimone JM, Samulsky ET. Superhydrophobic behavior of a perfluoropolyether lotus-leaf-like topography. Langmuir 2006;22(20):8576–80.
[38] Karapanogiotis I, Manoudis PN, Savva P, Panayiotou C. Superhydrophobic polymer-particle composite films produced using various particle sizes. Surf Interface Anal 2012;44(7):870–5.

[39] Manoudis PN, Karapanagiotis I. Modification of the wettability of polymer surfaces using nanoparticles. Prog Org Coat 2014;77(2):331–8.
[40] Shirtcliffe NJ, McHale G, Newton MI. The superhydrophobicity of polymer surfaces: recent developments. J Polym Sci Part B-Polym Phys 2011;49(17):1203–17.
[41] Nosonovsky M, Bhushan B. Biomimetic superhydrophobic surfaces: multiscale approach. Nano Lett 2007;7(9):2633–7.
[42] Miva M, Nakajima A, Fujishima A, Hashimoto K, Watanabe T. Effects of the surface roughness on sliding angles of water droplets on superhydrophobic surfaces. Langmuir 2000;16(13):5754–60.
[43] HDK – Pyrogenic silica. Available from: http://www.wacker.com/cms/media/publications/downloads/6180_EN.pdf.
[44] Gao LC, McCarthy TJ. A perfectly hydrophobic surface (theta(A)/theta(R)=180 degrees/180 degrees). J Am Chem Soc 2006;128(28):9052–3.
[45] Gao LC, McCarthy TJ. "Artificial lotus leaf" prepared using a 1945 patent and a commercial textile. Langmuir 2006;22(14):5998–6000.
[46] Wier KA, McCarthy TJ. Condensation on ultrahydrophobic surfaces and its effect on droplet mobility: ultrahydrophobic surfaces are not always water repellant. Langmuir 2006;22(6):2433–6.
[47] Gao LC, McCarthy TJ. Ionic liquids are useful contact angle probe fluids. J Am Chem Soc 2007;129(13). 3804-+.
[48] Gao LC, McCarthy TJ. How Wenzel and Cassie were wrong. Langmuir 2007;23(7):3762–5.
[49] Lee JA, McCarthy TJ. Polymer surface modification: topography effects leading to extreme wettability behavior. Macromolecules 2007;40(11):3965–9.
[50] Gao LC, Fadeev AY, McCarthy TJ. Superhydrophobicity and contact-line issues. Mrs Bull 2008;33(8):747–51.
[51] Gao LC, McCarthy TJ. Teflon is hydrophilic. Comments on definitions of hydrophobic, shear versus tensile hydrophobicity, and wettability characterization. Langmuir 2008;24(17):9183–8.
[52] Gao LC, McCarthy TJ. $(CH_3)(3)SiCl/SiCl_4$ azeotrope grows superhydrophobic nanofilaments. Langmuir 2008;24(2):362–4.
[53] Gao LC, McCarthy TJ. Wetting 101 degrees. Langmuir 2009;25(24):14105–15.
[54] Krumpfer JW, Bian P, Zhend PW, Gao LC, McCarthy TJ. Contact angle hysteresis on superhydrophobic surfaces: an ionic liquid probe fluid offers mechanistic insight. Langmuir 2011;27(6):2166–9.
[55] Krumpfer JW, McCarthy TJ. Dip-coating crystallization on a superhydrophobic surface: a million mounted crystals in a 1 cm(2) array. J Am Chem Soc 2011;133(15):5764–6.
[56] McCarthy M, Gerasopoulos K, Enright R, Culver JN, Ghodssi R, Wang EN. Biotemplated hierarchical surfaces and the role of dual length scales on the repellency of impacting droplets. Appl Phys Lett 2012;100(26).
[57] Bhushan B, Jung YC. Micro- and nanoscale characterization of hydrophobic and hydrophilic leaf surfaces. Nanotechnology 2006;17(11):2758–72.
[58] Nosonovsky M, Bhushan B. Biologically inspired surfaces: broadening the scope of roughness. Adv Funct Mater 2008;18(6):843–55.
[59] Bhushan B. Biomimetics: lessons from nature - an overview. Philos Trans R Soc a-Math Phys Eng Sci 2009;367(1893):1445–86.
[60] Koch K, Bhushan B, Barthlott W. Multifunctional surface structures of plants: an inspiration for biomimetics. Prog Mater Sci 2009;54(2):137–78.
[61] Wagner P, Furstner R, Barthlott W, Neinhuis C. Quantitative assessment to the structural basis of water repellency in natural and technical surfaces. J Exp Bot 2003;54(385):1295–303.
[62] Koch K, Neinhuis C, Ensikat HJ, Barthlott W. Self assembly of epicuticular waxes on living plant surfaces imaged by atomic force microscopy (AFM). J Exp Bot 2004;55(397):711–8.
[63] Furstner R, Barthlott W, Neinhuis C, Walzel P. Wetting and self-cleaning properties of artificial superhydrophobic surfaces. Langmuir 2005;21(3):956–61.
[64] Koch K, Hartmann KD, Schreiber L, Barthlott W, Neinhuis C. Influences of air humidity during the cultivation of plants on wax chemical composition, morphology and leaf surface wettability. Environ Exp Bot 2006;56(1):1–9.
[65] Ensikat HJ, Ditsche-Kuru P, Neinhuis C, Barthlott W. Superhydrophobicity in perfection: the outstanding properties of the lotus leaf. Beilstein J Nanotechnol 2011;2:152–61.
[66] Shirtcliffe NJ, McHale G, Newton MI, Perry JJ. Intrinsically superhydrophobic organosilica sol-gel foams. Langmuir 2003;19(14):5626–31.
[67] McHale G, Akil S, Shirtcliffe NJ, Newton MI, Erbil YH. Analysis of droplet evaporation on a superhydrophobic surface. Langmuir 2005;21(24):11053–60.
[68] Shirtcliffe NJ, McHale G, Newton MI, Perry JJ, Roach P. Porous materials show superhydrophobic to superhydrophilic switching. Chem Commun 2005;(25):3135–7.
[69] McHale G, Herbertson DL, Elliott SJ, Shirtcliffe NJ, Newton MI. Electrowetting of nonwetting liquids and liquid marbles. Langmuir 2007;23(2):918–24.
[70] McHale G, Newton MI, Shirtcliffe NJ. Dynamic wetting and spreading and the role of topography. J Phys Condens Matter 2009;21(46).
[71] Shirtcliffe NJ, McHale G, Newton MI. Learning from superhydrophobic plants: the use of hydrophilic areas on superhydrophobic surfaces for droplet control. Langmuir 2009;25(24):14121–8.
[72] Feng L, Li SH, Li YS, Li HJ, Zhang LJ, Shai J, et al. Super-hydrophobic surfaces: from natural to artificial. Adv Mater 2002;14(24):1857–60.
[73] Wagner T, Neinhuis C, Barthlott W. Wettability and contaminability of insect wings as a function of their surface sculptures. Acta Zool 1996;77(3):213–25.
[74] Byun D, Hong J, Ko JH, Lee YJ, Park HC, Byun BK, et al. Wetting characteristics of insect Wing surfaces. J Bionic Eng 2009;6(1):63–70.
[75] Yang C, Tartaglino U, Persson BNJ. Influence of surface roughness on superhydrophobicity. Phys Rev Lett 2006;97(11).